FEBS Letters

FEBS PRESS science publishing by scientists

Dual modulation of neuron-specific microRNAs and the REST complex promotes functional maturation of human adult induced neurons

Marcella Birtele[1], Yogita Sharma[1], Srisaiyini Kidnapillai[2], Shong Lau[1], Thomas B. Stoker[1,3], Roger A. Barker[1,3], Daniella Rylander Ottosson[1,2], Janelle Drouin-Ouellet[4] and Malin Parmar[1]

1 Department of Experimental Medical Science, Wallenberg Neuroscience Center, Division of Neurobiology, Lund Stem Cell Center, Lund University, Sweden
2 Regenerative Neurophysiology, BMC, Lund University, Sweden
3 Department of Clinical Neuroscience and WT-MRC Cambridge Stem Cell Institute, University of Cambridge, UK
4 Faculté de Pharmacie, Université de Montréal, Canada

Correspondence
M. Parmar, Wallenberg Neuroscience Center, Lund Stem Cell Center, Lund University, BMC A11, S-221 84 Lund, Sweden
Tel: +46 46 222 06 20
E-mail: malin.parmar@med.lu.se

Janelle Drouin-Ouellet and Malin Parmar contributed equally.

(Received 7 June 2019, revised 3 September 2019, accepted 8 September 2019)

doi:10.1002/1873-3468.13612

Edited by Holm Zaehres

The copyright line for this article was changed on 16 October 2019 after original online publication.

Direct neuronal reprogramming can be achieved using different approaches: by expressing neuronal transcription factors or microRNAs; and by knocking down neuronal repressive elements. However, there still exists a high variability in terms of the quality and maturity of the induced neurons obtained, depending on the reprogramming strategy employed. Here, we evaluate different long-term culture conditions and study the effect of expressing the neuronal-specific microRNAs, miR124 and miR9/9*, while reprogramming with forced expression of the transcription factors *Ascl1*, *Brn2*, and knockdown of the neuronal repressor REST. We show that the addition of microRNAs supports neuronal maturation in terms of gene and protein expression, as well as in terms of electrophysiological properties.

Keywords: direct reprogramming; electrophysiology; human adult neurons; induced neurons; miR124; miR9

Direct neuronal conversion, where a somatic cell is directly converted to an induced neuron (iN) [1], is an emerging alternative to induced pluripotent stem cells for disease modeling, diagnostics, drug screening, and cell replacement therapies. The main advantages of direct reprogramming include a fast route from fibroblast to the neuron of interest [2], the ability to gain cell-subtype specificity by altering the transcription factor (TF) combination [1,3–8], and the maintenance of the cellular phenotype associated with the age of the parental cell [9].

Neuronal reprogramming is most often achieved using defined combinations of TFs that are expressed

Abbreviations
AB-miR9/124, lentiviral vector containing Ascl1, Brn2, and miR9/9* and miR124; AB-shREST, lentiviral vector containing Ascl1, Brn2, and REST knockdown; AB-shREST-miR9/124, lentiviral vector containing Ascl1, Brn2, miR9/9* and miR124, and REST knockdown; APs, action potentials; Ascl1, achaete-scute homolog 1; Brn2, brain specific homeobox/POU domain protein 2; CIs, confidence intervals; CTR, control; DAPI, 4′,6-diamidino-2′-phenylindole dihydrochloride; DIV, days in vitro; DMEM, Dulbecco's modified Eagle's medium; iNs, induced neurons; MAP2, microtubule-associated protein 2; ORFs, open reading frames; PFL, polyornithine–fibronectin–laminin; REST, RE1-silencing transcription factor; RESTi, short hairpin-mediated knockdown of REST; RMP, resting membrane potential; shRNA, short hairpin RNA; TF, transcription factor.

during neuronal development. One of the most commonly used TFs is the proneuronal gene achaete-scute homolog 1 (*Ascl1*). *Ascl1* belongs to the family of the basic helix–loop–helix family, and it specifically binds DNA sequences containing an E-box motif [10]. Ascl1 alone can act as a pioneer factor occupying specific sites of the fibroblast genome [11]. Many other TFs can also contribute to the reprogramming, such as brain-specific homeobox/POU domain protein 2 (Brn2) that does not access fibroblast chromatin actively on their own but it is recruited by Ascl1 [11,12]. Also, microRNAs [13–16] and small molecules [17–20] have been shown to play a critical role in the conversion process. Overexpression of neuron-specific microRNA miR124 triggers a neuronal gene expression profile in a number of different cell types: HeLa cells, human embryonic carcinoma stem cells (NT2), mouse neuronal progenitor cells (N2A), human retinal epithelial cells (ARPE19), and primary mouse embryonic fibroblasts [21]. The forced expression of miR124 and another neuron-specific microRNA, miR9/9*, is sufficient for the cells converted from adult fibroblasts to adopt neuronal features [14]. Additionally, we have shown that while Ascl1 and Brn2 efficiently convert human fetal fibroblasts to neurons, human fibroblasts from adult donors require codelivery of miR9 and miR124 and/or knockdown of RE1-silencing TF (REST) [22]. The effect of short hairpin-mediated knockdown of REST (RESTi) on neuronal conversion efficiency is mediated at least in part *via* the upregulation of miR9 and miR124 as an effect of RESTi, but it is becoming clear that RESTi also acts *via* microRNA-independent pathways [22]. In line with this, it was shown that the combination of miR9/9* and miR124 can accelerate neuronal conversion [23,24]. However, the interplay between RESTi and neuron-specific miR9 and miR124 in morphological and functional maturation of iNs has yet to be fully understood.

Here, we report on a protocol for a long-term *in vitro* maturation that results in functionally mature iNs from dermal fibroblasts derived from elderly donors. Using this culture system, we have investigated the role of RESTi and its relation to miR9/9*-miR124 expression in the context of human iN maturation. Our results show that miR9/9*-miR124 adds to the effect of RESTi by promoting functional and morphological maturation of adult human iNs after several months in culture.

Materials and methods

Cell culture and cell lines

Adult dermal fibroblasts were obtained from the Parkinson's Disease Research Clinic at the John van Geest Centre for Brain Repair (Cambridge, UK) and used under local ethical approval (REC 09/H0311/88). For biopsy sampling information, see Drouin-Ouellet *et al.* [22]. Fibroblasts were expanded in T75 flasks with standard fibroblast medium [Dulbecco's modified Eagle's medium (DMEM), 10% FBS, 1% penicillin–streptomycin] at 37 °C in 5% CO_2. After thawing, cells were kept a minimum of 2 days in culture before starting experiments. When confluent, the cells were dissociated with 0.05% trypsin and plated at a lower density for expansion. To freeze the fibroblasts from a confluent T75 flask, the cells were detached after 5-min incubation in 0.05% trypsin at 37 °C, spun for 5 min at 400 g, and frozen in a 50/50 mixture of DMEM and FBS with 10% DMSO. The cell lines used in this study came from two healthy 67- and 70-year-old females at the time of skin sampling.

Viral vectors and virus transduction

In this study, the reprogramming protocol was applied using different combinations of lentiviral vectors. The DNA plasmids used are expressed in the open reading frames (ORFs) for *Ascl1*, *Brn2* with short hairpin RNA (shRNA) targeting REST or ORFs for *Ascl1*, *Brn2* with miRNA loops for miR9/9* and miR124 in combination with shRNA targeting REST. The lentiviruses used are third-generation vectors containing a nonregulated ubiquitous phosphoglycerate kinase promoter. The single vector containing *Ascl1*, *Brn2*, and shREST was used at MOI of 20 [22]. The vector containing *Ascl1*, *Brn2*, miR9/9*, and miR124 was used in combination with shRNA targeting REST at MOI 20. All viruses used in this study titered between 3×10^8 and 6×10^9 pfu·mL^{-1}.

Direct neuronal reprogramming

Fibroblasts were plated at a density of 27 800 cells·cm$-^2$ in 24-well plates (Nunc, Roskilde, Danmark). Prior to plating, the wells were coated overnight with a combination of PFL: polyornithine (15 μg·mL^{-1}), fibronectin (0.5 ng·μL^{-1}), and laminin (5 μg·mL^{-1}). Cells used for electrophysiological recordings were directly plated on glass coverslips coated with PFL. The following protocol, used for direct conversion, was previously described in Shrigley *et al.* [25] and Drouin-Ouellet *et al.* [22], with the omission of the replating step at day 12 of conversion for some of the experiments (see Results). Three days after the viral transduction, the fibroblast medium was replaced with neuronal differentiation medium (NDiff227; Takara-Clontech, Kusatsu, Shiga, Japan) supplemented with growth factors at the following concentrations: LM-22A4 (2 μM; R&D Systems, Minneapolis, MN, USA), GDNF (2 ng·mL^{-1}; R&D Systems), NT3 (10 ng·μL^{-1}; R&D Systems), and db-cAMP (0.5 mM; Sigma, St. Louis, MO, USA) and the small molecules CHIR99021

(2 μM; Axon, San Jose, CA, USA), SB-431542 (10 μM; Axon), noggin (0.5 $\mu g \cdot mL^{-1}$; R&D Systems), LDN-193189 (0.5 μM; Axon), and valproic acid sodium salt (1 mM; Merck Millipore, Burlington, MA, USA). Half-medium changes were performed every 2 days for the first 30 days of conversion, whereas in the later stages of conversion, the medium changes were done every 3 days. At 18 days post-transduction, the small molecules were withheld, and the neuronal medium was supplemented only with LM-22A4, GDNF, NT3, and db-cAMP until the end of the experiment.

Bioinformatics analyses

Fibroblasts were transduced with different lentiviral vectors (as in Drouin-Ouellet *et al.* [22]): AB, lentiviral vector containing *Ascl1*, *Brn2*, and miR9/9* and miR124 (AB-miR9/124), +/− shREST, and both untransduced fibroblasts and fibroblasts transduced only with REST shRNA were used as controls (CTR). Cells were cultured on gelatin until replating at day 10 [22]. iNs were collected for sequencing both at day 5 and at day 24 after transduction. RNA was extracted using miRNeasy Mini Kit (Qiagen, Hilden, Germany) with DNase treatment and sent for RNA sequencing to UCLA Clinical Microarray Core. cDNA libraries were prepared using the KAPA Stranded mRNA-Seq Kit from KAPA Biosystems. Single-end 50 base pair RNA sequencing sample reads were generated in one batch. The raw quality of reads was verified using Fastx toolkit and multiQC. The 50-bp single-end reads were mapped to the human genome assembly (GRCh38) using STAR mapper (2.4.0j) [26] with default parameters. mRNA expression was quantified using the subread package FeatureCounts [27] quantifying to NCBI annotation (GRCh38). Read counts were normalized to the total number of reads mapped to the genome. Mean–variance modeling and differential expression analysis were done using the voom/lmfit functions as implemented in the limma package [28]. Downstream analyses and visualizations were performed using the in-house R scripts (Vienna, Austria).

RT-qPCR for neuronal gene expression

Total RNA was extracted using the miRNeasy Kit (Qiagen), followed by cDNA synthesis using Universal cDNA Synthesis Kit (Thermo Fisher Scientific, Waltham, MA, USA). Three reference genes were used for each qPCR analysis (*Actb*, *Gapdh*, and *Hprt1*). All primers were used together with LightCycler 480 SYBR Green I Master (Roche, Basel, Switzerland). Standard procedures of qRT-PCR were used and data quantified using the $\Delta\Delta C_t$ method. Statistical analyses were performed in triplicates. A custom RT^2 Profiler PCR Array (Qiagen) containing 90 neuronal genes was also used in gene expression analysis according to the manufacturer's instructions.

Whole-cell patch-clamp recording

Prior to recording, cells on glass coverslips were transferred from the NDiff227 medium (supplemented with LM-22A4, GDNF, NT3, and db-cAMP) to BrainPhys media [29] for 30 mins in order to promote the maintenance and prepare the cells for electrophysiological recordings. Cells were then moved to a recording chamber and submerged in a flowing artificial cerebrospinal fluid (ACSF) solution gassed with 95% O_2 and 5% CO_2 at 23 °C according to the standard procedures for recording. The composition of the ACSF was as follows (in mM): 126 NaCl, 2.5 KCl, 1.2 NaH_2PO_4–H_2O, 1.3 $MgCl_2$–$6H_2O$ and 2.4 $CaCl_2$–$6H_2O$, 22 $NaHCO_3$, and 10 glucose. The pH of the solution was adjusted to 7.4. The temperature of the chamber was maintained at 34 °C throughout the entire recording session. Multiclamp 700B (Molecular Devices, San Jose, CA, USA) was used for recordings, and signals were acquired at 10 kHz using pCLAMP10 software and a data acquisition unit (Digidata 1440A; Molecular Devices). Input resistances and injected currents were monitored throughout the experiments. Borosilicate glass pipettes (4–7 MΩ) for patching were filled with the following intracellular solution (in mM): 122.5 potassium gluconate, 12.5 KCl, 0.2 EGTA, 10 HEPES, 2 MgATP, 0.3 Na_3GTP, and 8 NaCl. Solution was adjusted to pH 7.3 with KOH as in Ref. [4]. Resting membrane potentials (RMP) were monitored immediately after breaking-in in current-clamp mode. Membrane capacitance was monitored throughout the recordings, and recordings were discarded if changes in values higher than 30% were observed. Membrane potential was kept between −60 and −70 mV, and currents were injected from −20 to +90 pA with 10 pA increments to induce action potentials (APs). Inward sodium and delayed rectifying potassium currents were measured in voltage clamp at depolarizing steps of 10 mV.

Immunocytochemistry, imaging, and high-content screening analysis

Fixation of the cells was done with 4% paraformaldehyde, followed by 10 min of permeabilization with 0.1% Triton X-100 in 0.1 M phosphate base saline, PBS. Cells were blocked for 30 min in 5% normal serum diluted in 0.1 M PBS. In the same blocking solution, the primary antibodies were diluted as follows: rabbit anti-microtubule-associated protein 2 (MAP2; 1 : 500; Millipore) and mouse anti-TAU (1 : 500; Invitrogen Antibodies, Waltham, MA, USA). Each 24-well plate was incubated overnight with 0.5 mL of primary antibody solution at 4 °C. After two washes with PBS, the cells were left in blocking solution at room temperature together with fluorophore-conjugated secondary antibodies (Jackson ImmunoResearch Laboratories, Ely, UK) for at least 2 h. Cells were then stained with 4′,6-diamidino-2′-phenylindole dihydrochloride (DAPI; 1 : 1000; Sigma-Aldrich) for 15 min at RT followed by three washes

with PBS. Cells were analyzed with the Cellomics Array Scan (Array Scan VTI; Thermo Fisher Scientific, Waltham, MA, USA) using the two bioapplications: 'Target Activation' and 'Neuronal Profiling'. The total number of MAP2- and TAU-positive cells with a neuronal morphology was also estimated by manual counting of 36 fields of view that were randomly chosen at a 20× magnification, as previously described in Ref. [4]. This procedure was repeated 3×, and the average number was used to derive the total number of neurons in the wells. Digital images were obtained from a Leica microscope (Wetzlar, Germany).

Statistical analysis

All data are expressed as mean ± the standard error of the mean or mean ± confidence intervals (CIs). Statistical analyses were done using the GRAPHPAD PRISM 7.0 (San Diego, CA, USA). An alpha level of $P < 0.05$ was set for significance. Groups were compared using a one-way or two-way ANOVA followed by a Bonferroni *post hoc* analysis. In the case of only two groups, Student's *t*-test was performed.

Results

Transcriptional profiling reveals a potential early role for miR9/124 in neuronal maturation

In order to elucidate the role and possible synergistic effect of RESTi and miRNAs during different stages of reprogramming, we performed global gene expression analysis of adult fibroblasts converted with *Ascl1*, *Brn2*, and RESTi (AB-shREST) at 5 and 24 days postconversion and compared that to the gene expression in cells converted using miR9 and miR124 in addition to *Ascl1*, *Brn2*, and RESTi (AB-shREST-miR9/124). As we previously reported, there were no major changes in gene expression between the two conversion conditions 5 days after the initiation of conversion (Fig. 1A and Table S1; Ref. [22]). However, we found that a few genes associated with calcium signaling (*CACNG8*, *TNNT1*, *PALM3*) were more highly expressed in the AB-shREST-miR9/124 group (Fig. 1A), which prompted us to perform the transcriptome analysis also 24 days after conversion. At this stage, we found that there was more divergent gene expression between the microRNA- and non-microRNA-reprogrammed cells (Fig. 1B and Table S2). When comparing the gene expression of AB-shREST-miR9/124 group between days 5 and 24, we found that many genes associated with neuronal maturation and function were upregulated at day 24 (Fig. 1C and Table S3). The average gene expression analysis between day 5 and day 24 showed that some of the genes that are related to neuronal differentiation and neuronal maturation, such as *POU3F2*, *NPTX1*, *RIMS4*, and *C1QL*, were more highly expressed in iNs reprogrammed with the addition of miR9/124 (Fig. 1C). When targeting the analysis on synaptic or ion channel-related genes, we found that *SNAP29*, *PFN2*, and *FGF12* were increased significantly in the differential expression between AB-shREST-miR9/124 vs AB-shREST at day 24. Also, other synaptic genes, such as *SYT1*, showed a trend of higher expression at day 24 vs day 5 (Fig. 1D). Electrophysiological recordings were performed at 24 days (Fig. 1E) in order to see whether this increase in mature gene expression also resulted in more mature functional properties of the cells. We recorded RMP (Fig. 1F), inward/outward currents (Fig. 1G), current-induced APs (Fig. 1H), and spontaneous firing (Fig. 1I) in each condition. However, there were no signs of physiological neuronal maturation at this time point with either conversion methods (Fig. 1F–I and Table S4). This suggests that despite some differences in the expression of genes related to neuronal maturation and synaptic function between the two conditions, none of the conditions generated cells with mature functional properties at this relatively early time point. Thus, culture conditions that allow for long-term survival, attachment, and maturation are needed for functional assessments of iNs.

Polyornithine–fibronectin–laminin coating is optimal for long-term culture of human adult iNs

To allow for studies on how shREST and miR9/124 expressions affect neuronal maturation and function over time, we set out to establish a system optimized for long-term culturing that is permissive for functional maturation of iNs under reductionist conditions without the need for feeder layers (see Fig. 2A for experimental overview). First, we evaluated four different coating conditions (Fig. 2B): gelatin, laminin 111, Matrigel, PFL for their capacity to support the cell attachment and survival for an extended time *in vitro*. When quantified, we could not detect a difference in conversion efficiencies (Fig. 2C). When screening coating conditions that allow attachment of a large number of iNs, conversions were either initiated directly on the different coating conditions or initiated on gelatin, then were replated from gelatin onto the different coatings after 12 days (Fig. 2A). Quantification of the number of iNs in each condition showed that Matrigel and PFL best support iN generation and that omitting the replating step was beneficial (Fig. 2D vs 2E). When analyzing cells after replating, we noticed a similar trend for the Matrigel and PFL conditions (Fig. 2E). However, we failed to obtain a good cell attachment

after replating in several experiments, which precluded statistical analysis. Based on this, we decided to proceed with the PFL coating without a replating step and confirmed good attachment, cell viability, and morphological maturation after 60 days of culturing (Fig. 2F).

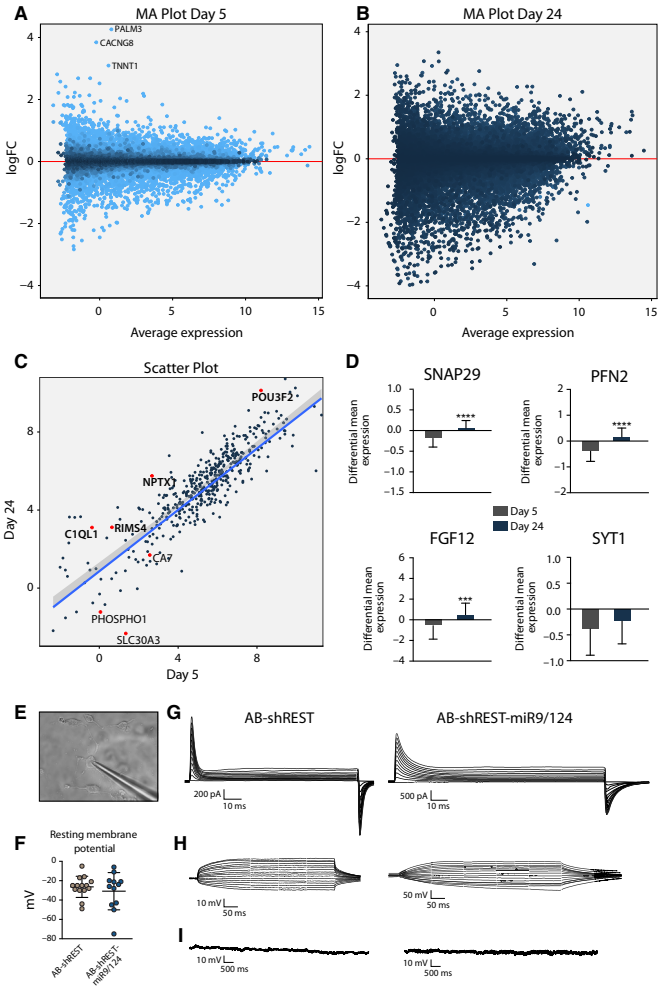

Fig. 1. Differential gene expression in iNs converted with AB-shREST-miR9/124 vs AB-shREST. (A) MA plot at day 5 indicating average gene expression of the samples AB-shREST-miR9/124 (n = 3) compared to AB-shREST (n = 3). At this time point, genes related to ion and calcium regulation such as *PALM3*, *CACNG8,* and *TNNT1* were found to be upregulated in the AB-shREST-miR9/124 condition. (B) MA plot at day 24 indicating average gene expression of the samples AB-shREST-miR9/124 (n = 3) compared to AB-shREST (n = 3). At this time point, the general high divergence of gene expression can be found in between the conditions. (C) Scatter plot of top genes at day 5 and day 24 indicating an upregulation of the neuronal genes *POU3F2*, *NPTX1*, *RIMS4, and C1QL* in AB-shREST-miR9/124 sample. (D) Plots of differential expression for genes related to neuronal maturation and function such as *SNAP29*, *FGF12*, *SYT1*, and *PFN2* in AB-shREST-miR9/124 samples at day 5 and day 24. Plots show an increase in these genes at day 24 in AB-shREST-miR9/124-converted cells. Analysis performed with two-way ANOVA and multiple comparison analysis with the Bonferroni *post hoc* correction. **** $P < 0.0001$, *** $P = 0.003$. Graphs showing mean values and relative CI. All transcriptional analyses (A–D) were performed using data from biological replicates (n = 3) for each group. (E) Example of whole-cell patch-clamp recording performed on AB-shREST and AB-shREST-miR9/124 conditions at day 24. (F) Plot of RMP values from AB-shREST condition and AB-shREST-miR9/124 condition. Values show immature RMP for both conditions. Plots indicating the mean of RMP and relative SEM calculated from Student's t-test analysis. (G) Examples of inward sodium/outward potassium currents from whole-cell patch-clamp recordings for AB-shREST condition (left panel) and AB-shREST-miR9/124 condition (right panel). All recordings showed an absence of currents. (H) Examples of induced APs from whole-cell patch-clamp recordings for AB-shREST condition (left panel) and AB-shREST-miR9/124 condition (right panel). All recordings showed an absence of induced APs. (I) Examples of spontaneous firing from whole-cell patch-clamp recordings for AB-shREST condition (left panel) and AB-shREST-miR9/124 condition (right panel). All recordings showed an absence of activity. Electrophysiological recordings (E–I) were performed on AB-shREST condition (n = 14 recorded cells) and AB-shREST-miR9/124 condition (n = 12 recorded cells). MA: M (log ratio) and A (mean average); logFC: logarithmic fold changes; SEM: standard error of the mean.

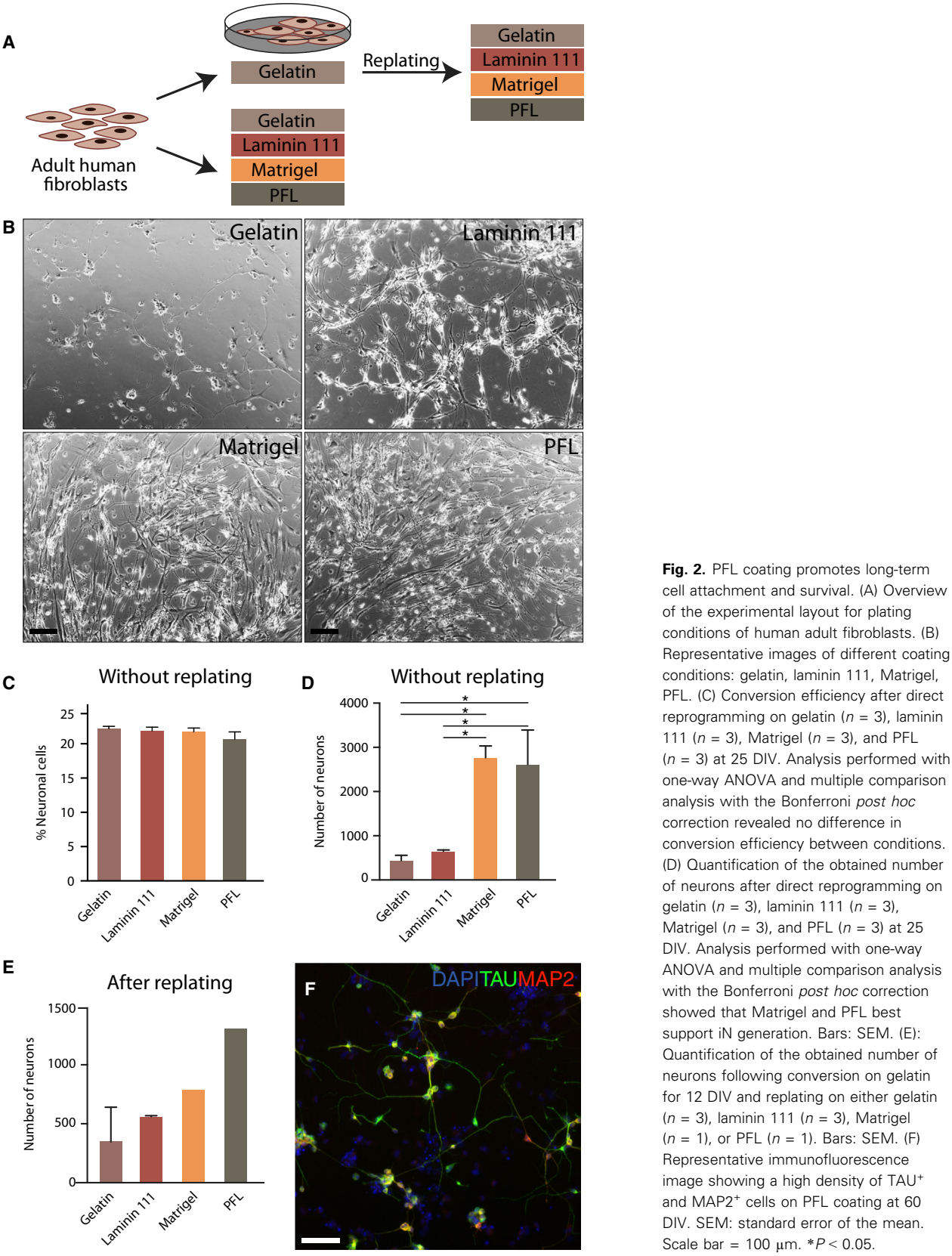

Fig. 2. PFL coating promotes long-term cell attachment and survival. (A) Overview of the experimental layout for plating conditions of human adult fibroblasts. (B) Representative images of different coating conditions: gelatin, laminin 111, Matrigel, PFL. (C) Conversion efficiency after direct reprogramming on gelatin (n = 3), laminin 111 (n = 3), Matrigel (n = 3), and PFL (n = 3) at 25 DIV. Analysis performed with one-way ANOVA and multiple comparison analysis with the Bonferroni *post hoc* correction revealed no difference in conversion efficiency between conditions. (D) Quantification of the obtained number of neurons after direct reprogramming on gelatin (n = 3), laminin 111 (n = 3), Matrigel (n = 3), and PFL (n = 3) at 25 DIV. Analysis performed with one-way ANOVA and multiple comparison analysis with the Bonferroni *post hoc* correction showed that Matrigel and PFL best support iN generation. Bars: SEM. (E): Quantification of the obtained number of neurons following conversion on gelatin for 12 DIV and replating on either gelatin (n = 3), laminin 111 (n = 3), Matrigel (n = 1), or PFL (n = 1). Bars: SEM. (F) Representative immunofluorescence image showing a high density of TAU^+ and $MAP2^+$ cells on PFL coating at 60 DIV. SEM: standard error of the mean. Scale bar = 100 μm. $*P < 0.05$.

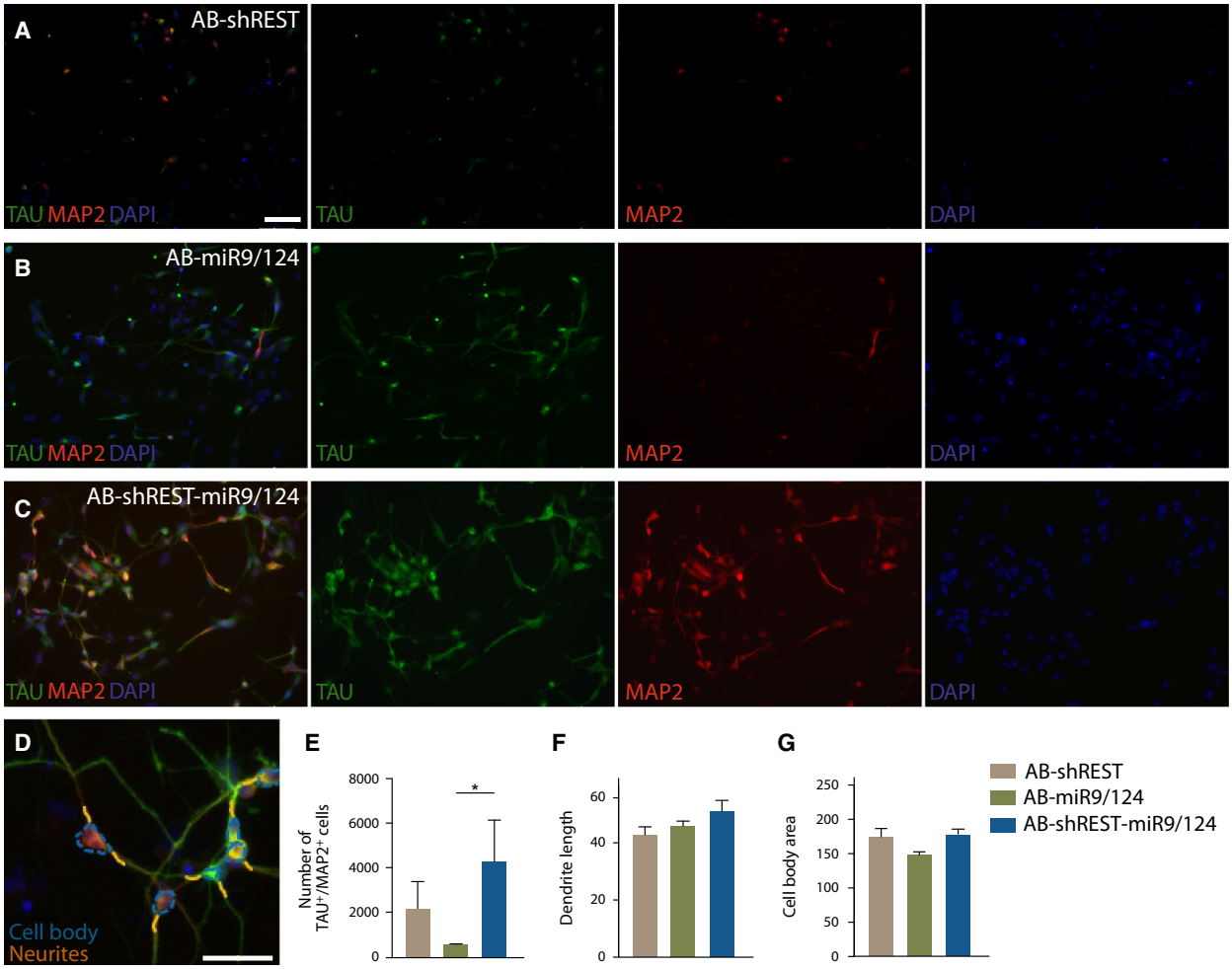

Fig. 3. Conversion efficiency and morphological maturation of reprogrammed human adult neurons. (A–C) Representative images of DAPI/TAU$^+$/MAP2$^+$ iNs at 24 DIV. (D) Example of cell body and neurite detection using a high-content screening analysis. (E) Quantification of the number of the DAPI/TAU$^+$/MAP2$^+$ (n = 3 in each condition). Statistical analysis performed using one-way ANOVA with the Bonferroni *post hoc* correction revealed that AB-shREST-miR9/124 conversion showed a highest number of neurons. *$P < 0.05$. (F) Quantification of neurite length (n = 3 in each condition). Statistical analysis was performed using one-way ANOVA with the Bonferroni *post hoc* correction, no differences between the conditions were detected. (G) Quantification of cell body area (n = 3 in each condition). Statistical analysis was performed using one-way ANOVA with the Bonferroni *post hoc* correction, no differences between the conditions were detected. Error bars: SEM. SEM: standard error of the mean. Scale bar = 75 μm.

With the conditions for long-term cultures optimized, we next compared neuronal maturation of cells converted using either the AB-shREST or AB-shREST-miR9/124 conditions in long-term cultures on PFL.

Increase in mature neuronal marker expression and electrophysiological properties over time in iNs converted using a combination of shREST and miR9/124

We first investigated the morphological differences between cells converted with the AB-shREST or AB-shREST-miR9/124. We also included cells converted in the presence of miR9/124 but not shREST (AB-miR9/124). To investigate the effect on conversion efficiency and potential differences in morphology between the groups, cultures were stained for TAU and MAP2, two microtubule-associated proteins expressed in mature neurons (Fig. 3A–C). Quantification of the number of cells that expressed both TAU and MAP2 was performed with automated and unbiased high-content screening (Cellomics; Fig. 3D). The analysis showed that while AB-shREST and AB-miR9/124 reprogrammed iNs with a similar efficiency, the highest number of neurons that had matured to express these two proteins was detected when cells

were converted with miR9/miR124 together with shREST (Fig. 3E). The combined AB-shREST-miR9/124 conditions also displayed a trend toward having longer neurites (Fig. 3F), while the cell body area appeared to be similar among all conditions (Fig. 3G). This result is in line with the bioinformatics data, showing that at this stage of reprogramming, iNs are expressing mature neuronal markers of the cytoskeleton but are not yet electrophysiologically functional.

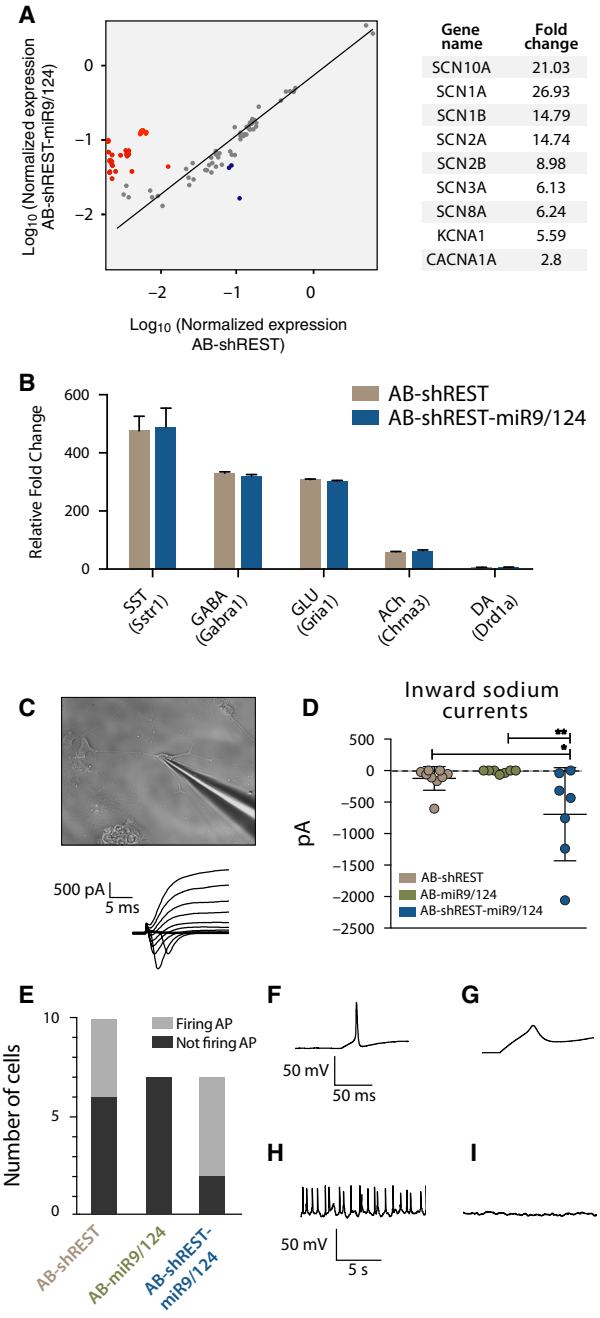

Next, we analyzed the effect of miR9/miR124 and shREST on functional maturation at a later stage of the reprogramming process. We first performed an extensive gene expression analysis targeted to detect relevant genes of neuronal functions (neuronal ion channels) after 90 days in culture. Here, we found an upregulation of 10 genes related to voltage-gated sodium channels in the AB-shREST-miR9/124 condition compared to AB-shREST condition (Fig. 4A), suggesting a more mature neuronal phenotype when miR9/124 has been added. When looking for specific neurotransmitter phenotypes, cells showed a similar expression of somatostatin-, GABAergic-, glutamatergic-, acetylcholinergic-, and dopaminergic-related genes (*SSTR1*, *GABRA1*, *GRIA2, CHRMA43*, and *DRD1;* Fig. 4B). To further assess the functional maturation, iNs converted using the different conditions were recorded after 80–85 days *in vitro* (DIV) and using whole-cell patch-clamp technique. Neuronal-like cells were identified based on morphology (cell body shape, presence of protrusions, and dendrites) in the cultures and targeted with microelectrodes for single-cell electrophysiological recordings (Fig. 4C, upper picture). Monitoring of the passive membrane properties was performed in order to compare iNs among the different conditions (Table S5). In voltage-clamp mode, we checked the presence of inward sodium and outward potassium currents in all the cells as a measure of the

Fig. 4. Whole-cell patch-clamp recordings of iNs converted with different vectors at 80 DIV. (A) Fold change of the top upregulated neuronal and ion channel-related genes in AB-shREST-miR9/124 as compared to AB-shREST. Significantly up- and downregulated genes are in red and blue, respectively. (B) Relative fold change expression for specific genes such as *SSTR1*, *GABRA1*, *GRIA1*, *CHRNA3,* and *DRD1* indicating similar expression of neuronal subtype generated in both AB-shREST1 ($n = 3$) and AB-shREST-miR9/124 ($n = 3$) conditions. Statistical analysis was performed using Student's *t*-test, no differences between the conditions were detected. (C) Representative image of a patched iN and representative inward sodium/outward potassium electrophysiological recording of iNs reprogrammed using AB-shREST1-miR9/124. (D) Quantification of Inward sodium current (AB-shREST, $n = 9$; AB-miR9/124, $n = 7$; AB-shREST-miR9/124, $n = 7$). Analysis performed using one-way ANOVA with the Bonferroni *post hoc* correction revealed higher sodium currents in AB-shREST-miR9/124 condition. (E) Quantification of the number of cells firing APs in each group (AB-shREST, $n = 9$; AB-miR9/124, $n = 7$; AB-shREST-miR9/124, $n = 7$). (F) Example of mature induced AP in an iN cell reprogrammed using AB-shREST1-miR9/124. (G) Example of immature induced AP present in an iN cell reprogrammed using AB-shREST. (H) Example of spontaneous firing present in the group AB-shREST-miR9/124. (I) Absence of spontaneous firing in the group AB-miR9/124.

expression of voltage-gated sodium and potassium channels (Fig. 4C, lower). The currents for each group of conversion were analyzed and revealed that no, or only a few, cells showing the presence of inward sodium currents were present in the group of cells converted with AB-shREST and AB-miR9/124, whereas the majority of iNs converted with AB-shREST-miRNA124/9 showed inward currents (Fig. 4D). The iNs reprogrammed using AB-shREST-miRNA124/9 also showed more mature membrane properties. In current-clamp mode, steps of currents were injected in the cells in order to detect their ability to generate APs. Conversion with AB-shREST-miR9/124 resulted in a higher proportion of cells capable of firing current-induced APs (Fig. 4E). Furthermore, the APs generated were of higher amplitude in this group (Fig. 4F), indicating a greater maturation level in comparison with cells reprogrammed with miR9/124 or shREST only, in which only immature APs were detected (Fig. 4G). In these iNs, the presence of spontaneous firing was detected in current mode (Fig. 4H), indicating that the maturation level in this group was higher compared to the reprogramming conditions with miR9/124 or shREST only, where mostly spontaneous firing was absent (Fig. 4I).

Discussion

Induced neurons can be used for disease modeling, diagnostics, and drug screening [2,30,31]. As the technology becomes more and more refined, the use of iNs to model neurological diseases is increasing. However, while conversion of human fetal fibroblasts has been reported in a growing number of studies [3,4,7,32,33], only a few studies to date have shown high levels of neuronal conversion of fibroblasts from aged individuals [9,22]. New protocols that allow for the conversion of adult fibroblasts involve shREST [25] and/or microRNA delivery [14,16]. While it is clear that both these modulations greatly improve conversion efficiency, their relative contribution to neuronal maturation is less clear.

In this study, we report a conversion protocol optimized for long-term culturing of human iNs that allows for morphological and functional assessments after long-term culture *in vitro* under reductionistic conditions in the absence of feeders. When comparing iNs converted in the presence of shREST and/or miR9/124 over time using this protocol, we made a number of interesting observations. The quantification of iNs and comparative transcriptional profiling of the cells at 5 and 24 days after initiation of conversion indicated that while the addition of miRNAs during the conversion does not increase the neuronal yield, it does result in increased expression of genes associated with neuronal function. Already at 24 days, this resulted in more mature iNs although they were not functional at this time point. Interestingly, when the functional properties of the iNs were assessed after several more weeks of culturing *in vitro*, we found that boosting miRNA expression in addition to gene delivery and RESTi did not affect the subtype identity of the neurons, but was beneficial for functional maturation of iNs. Thus, while the expression of miR9 and miR124 initiated *via* shREST is sufficient for successful conversion using Ascl1 and Brn2 as conversion factors (this study and in Ref. [22]), further boosting miRNA expression *via* viral delivery results in increased expression of genes associated with synaptic function and ion channels, and also results in accelerated functional maturation. This lays the foundation for long-term studies of neuronal functions and disease-associated dysfunctions in patient-derived iNs.

The long-term culture protocol that allows for robust functional maturation of iNs *in vitro* presented here (Fig. 2A) opens up the possibility of modeling disease-related properties that develop over several months in culture, such as synaptic dysfunction, protein aggregation, and increased sensitivity to environmental factors. Our data also suggest that functional maturation can, at least in part, be controlled separately from neuronal specification during iN conversion. Supporting this, increased and accelerated maturation *via* external factors during iN conversion can also be achieved *via* the constitutive expression of SMAD3 [17,34,35]. We anticipate that these findings, as well as continued studies seeking to identify molecular regulators of neuronal maturation, will enable more refined and possibly accelerated studies of disease-related functional properties *in vitro*.

Acknowledgements

We thank Marie Persson Vejgården and Sol Da Rocha Baez for technical assistance and Dr. Anna Hammarberg for her valuable help with high-content screening. We also thank Petter Storm for the help with the bioinformatics analysis. The research leading to these results has received funding from the European Research Council under the European Union's Seventh Framework Programme: FP/2007-2013 NeuroStemcellRepair (no. 602278) and ERC Grant Agreement no. 30971, the Swedish Research Council (grant agreement 521-2012-5624 and 70862601/ Bagadilico), Swedish Parkinson Foundation

(Parkinsonfonden), and the Strategic Research Area at Lund University Multipark (Multidisciplinary Research in Parkinson's Disease). Marcella Birtele is supported by a BMT MarieCurie Horizon 2020 fellowship. J. D.-O. is receiving salary support from the Fonds du Québec en Recherche, Santé (FRQS) and Parkinson Québec.

Conflict of interest

MP is the owner of Parmar Cells AB and co-inventor of the U.S. patent application 15/093,927 owned by BioLamina AB and EP17181588 owned by Miltenyi Biotec.

Data availability

Raw counts for day 5 data were downloaded from GEO submission ID GSE90068. The RNA-Seq dataset for day 25 can be found on the GEO repository under accession number GSE132154.

Author contributions

MB, JD-O, and MP conceived and designed experiments; MB YS, SK, and SL, performed experiments and analyzed data; TBS and RAB provided cells and materials; DRO provided expertise in electrophysiological analysis; MB, JD-O, and MP wrote the manuscript; all authors provided input and comments on the manuscript.

References

1 Vierbuchen T, Ostermeier A, Pang ZP, Kokubu Y, Südhof TC and Wernig M (2010) Direct conversion of fibroblasts to functional neurons by defined factors. *Nature* **463**, 1035–1041.

2 Yang N, Ng YH, Pang ZP, Südhof TC and Wernig M (2011) Induced neuronal cells: how to make and define a neuron. *Cell Stem Cell* **9**, 517–25.

3 Caiazzo M, Dell'Anno MT, Dvoretskova E, Lazarevic D, Taverna S, Leo D, Sotnikova TD, Menegon A, Roncaglia P, Colciago G *et al.* (2011) Direct generation of functional dopaminergic neurons from mouse and human fibroblasts. *Nature* **476**, 224–227.

4 Pfisterer U, Kirkeby A, Torper O, Wood J, Nelander J, Dufour A, Bjorklund A, Lindvall O, Jakobsson J and Parmar M (2011) Direct conversion of human fibroblasts to dopaminergic neurons. *Proc Natl Acad Sci USA* **108**, 10343–10348.

5 Wainger BJ, Buttermore ED, Oliveira JT, Mellin C, Lee S, Saber WA, Wang AJ, Ichida JK, Chiu IM, Barrett L *et al.* (2015) Modeling pain *in vitro* using nociceptor neurons reprogrammed from fibroblasts. *Nat Neurosci* **18**, 17–24.

6 Blanchard JW, Eade KT, Szűcs A, Lo Sardo V, Tsunemoto RK, Williams D, Sanna PP and Baldwin KK (2015) Selective conversion of fibroblasts into peripheral sensory neurons. *Nat Neurosci* **18**, 25–35.

7 Son EY, Ichida JK, Wainger BJ, Toma JS, Rafuse VF, Woolf CJ and Eggan K (2011) Conversion of mouse and human fibroblasts into functional spinal motor neurons. *Cell Stem Cell* **9**, 205–218.

8 Liu X, Li F, Stubblefield EA, Blanchard B, Richards TL, Larson GA, He Y, Huang Q, Tan A-C, Zhang D *et al.* (2012) Direct reprogramming of human fibroblasts into dopaminergic neuron-like cells. *Cell Res* **22**, 321–332.

9 Mertens J, Paquola ACM, Ku M, Hatch E, Böhnke L, Ladjevardi S, McGrath S, Campbell B, Lee H, Herdy JR *et al.* (2015) Directly reprogrammed human neurons retain aging-associated transcriptomic signatures and reveal age-related nucleocytoplasmic defects. *Cell Stem Cell* **17**, 705–718.

10 Bertrand N, Castro DS and Guillemot F (2002) Proneural genes and the specification of neural cell types. *Nat Rev Neurosci* **3**, 517–530.

11 Wapinski OL, Lee QY, Chen AC, Li R, Corces MR, Ang CE, Treutlein B, Xiang C, Baubet V, Suchy FP *et al.* (2017) Rapid chromatin switch in the direct reprogramming of fibroblasts to neurons. *Cell Rep* **20**, 3236.

12 Wapinski OL, Vierbuchen T, Qu K, Lee QY, Chanda S, Fuentes DR, Giresi PG, Ng YH, Marro S, Neff NF *et al.* (2013) Hierarchical mechanisms for direct reprogramming of fibroblasts to neurons. *Cell* **155**, 621–635.

13 Ambasudhan R, Talantova M, Coleman R, Yuan X, Zhu S, Lipton SA and Ding S (2011) Direct reprogramming of adult human fibroblasts to functional neurons under defined conditions. *Cell Stem Cell* **9**, 113–118.

14 Yoo AS, Sun AX, Li L, Shcheglovitov A, Portmann T, Li Y, Lee-Messer C, Dolmetsch RE, Tsien RW and Crabtree GR (2011) MicroRNA-mediated conversion of human fibroblasts to neurons. *Nature* **476**, 228–31.

15 Victor MB, Richner M, Hermanstyne TO, Ransdell JL, Sobieski C, Deng P-Y, Klyachko VA, Nerbonne JM and Yoo AS (2014) Generation of human striatal neurons by MicroRNA-dependent direct conversion of fibroblasts. *Neuron* **84**, 311–323.

16 Abernathy DG, Kim WK, McCoy MJ, Lake AM, Ouwenga R, Lee SW, Xing X, Li D, Lee HJ, Heuckeroth RO *et al.* (2017) MicroRNAs induce a permissive chromatin environment that enables neuronal subtype-specific reprogramming of adult human fibroblasts. *Cell Stem Cell* **21**, 332–348.e9.

17 Ladewig J, Mertens J, Kesavan J, Doerr J, Poppe D, Glaue F, Herms S, Wernet P, Kögler G, Müller F-J *et al.* (2012) Small molecules enable highly efficient neuronal conversion of human fibroblasts. *Nat Methods* **9**, 575–578.
18 Liu M-L, Zang T, Zou Y, Chang JC, Gibson JR, Huber KM and Zhang C-L (2013) Small molecules enable neurogenin 2 to efficiently convert human fibroblasts into cholinergic neurons. *Nat Commun* **4**, 2183.
19 Pfisterer U, Ek F, Lang S, Soneji S, Olsson R and Parmar M (2016) Small molecules increase direct neural conversion of human fibroblasts. *Sci Rep* **6**, 38290.
20 Smith DK, Yang J, Liu M-L and Zhang C-L (2016) Small molecules modulate chromatin accessibility to promote NEUROG2-mediated fibroblast-to-neuron reprogramming. *Stem Cell Reports* **7**, 955–969.
21 Xue Y, Ouyang K, Huang J, Zhou Y, Ouyang H, Li H, Wang G, Wu Q, Wei C, Bi Y *et al.* (2013) Direct conversion of fibroblasts to neurons by reprogramming PTB-regulated microRNA circuits. *Cell* **152**, 82.
22 Drouin-Ouellet J, Lau S, Brattås PL, Rylander Ottosson D, Pircs K, Grassi DA, Collins LM, Vuono R, Andersson Sjöland A, Westergren-Thorsson G *et al.* (2017) REST suppression mediates neural conversion of adult human fibroblasts via microRNA-dependent and -independent pathways. *EMBO Mol Med* **9**, 1117–1131.
23 Xue Y, Qian H, Hu J, Zhou B, Zhou Y, Hu X, Karakhanyan A, Pang Z and Fu X-D (2016) Sequential regulatory loops as key gatekeepers for neuronal reprogramming in human cells. *Nat Neurosci* **19**, 807–815.
24 Wohl SG and Reh TA (2016) miR-124-9-9* potentiates Ascl1-induced reprogramming of cultured Müller glia. *Glia* **64**, 743–62.
25 Shrigley S, Pircs K, Barker RA, Parmar M and Drouin-Ouellet J (2018) Simple generation of a high yield culture of induced neurons from human adult skin fibroblasts. *J Vis Exp* e56904, https://doi.org/10.3791/56904.
26 Dobin A, Davis CA, Schlesinger F, Drenkow J, Zaleski C, Jha S, Batut P, Chaisson M and Gingeras TR (2013) STAR: ultrafast universal RNA-seq aligner. *Bioinformatics* **29**, 15–21.
27 Liao Y, Smyth GK and Shi W (2014) featureCounts: an efficient general purpose program for assigning sequence reads to genomic features. *Bioinformatics* **30**, 923–930.
28 Ritchie ME, Phipson B, Wu D, Hu Y, Law CW, Shi W and Smyth GK (2015) limma powers differential expression analyses for RNA-sequencing and microarray studies. *Nucleic Acids Res* **43**, e47. https://doi.org/10.1093/nar/gkv007.
29 Bardy C, Van Den Hurk M, Eames T, Marchand C, Hernandez RV, Kellogg M, Gorris M, Galet B, Palomares V, Brown J *et al.* (2015) Neuronal medium that supports basic synaptic functions and activity of human neurons in vitro. *Proc Natl Acad Sci USA* **112**, E2725–E2734. https://doi.org/10.1073/pnas.1504393112.
30 Fang L, El Wazan L, Tan C, Nguyen T, Hung SSC, Hewitt AW and Wong RCB (2018) Potentials of cellular reprogramming as a novel strategy for neuroregeneration. *Front Cell Neurosci* **12**, 460.
31 Drouin-Ouellet J, Pircs K, Barker RA, Jakobsson J and Parmar M (2017) Direct neuronal reprogramming for disease modeling studies using patient-derived neurons: what have we learned? *Front Neurosci* **11**, 530.
32 Miskinyte G, Devaraju K, Grønning Hansen M, Monni E, Tornero D, Woods NB, Bengzon J, Ahlenius H, Lindvall O and Kokaia Z (2017) Direct conversion of human fibroblasts to functional excitatory cortical neurons integrating into human neural networks. *Stem Cell Res Ther* **8**, 207.
33 Pang ZP, Yang N, Vierbuchen T, Ostermeier A, Fuentes DR, Yang TQ, Citri A, Sebastiano V, Marro S, Südhof TC *et al.* (2011) Induction of human neuronal cells by defined transcription factors. *Nature* **476**, 220–223.
34 Ruetz T, Pfisterer U, Di Stefano B, Ashmore J, Beniazza M, Tian TV, Kaemena DF, Tosti L, Tan W, Manning JR *et al.* (2017) Constitutively active SMAD2/3 are broad-scope potentiators of transcription-factor-mediated cellular reprogramming. *Cell Stem Cell* **21**, 791–805.e9.
35 Pereira M, Pfisterer U, Rylander D, Torper O, Lau S, Lundblad M, Grealish S and Parmar M (2014) Highly efficient generation of induced neurons from human fibroblasts that survive transplantation into the adult rat brain. *Sci Rep* **4**, 6330.

Supporting information

Additional supporting information may be found online in the Supporting Information section at the end of the article.

Table S1. Raw data for differential expression analysis at day 5.

Table S2. Raw data for differential expression analysis at day 24.

Table S3. Normalized counts files of gene expression at day 5 and day 24.

Table S4. Passive electrical properties of cell membranes from Whole-cell patch-clamp recordings at day 24.

Table S5. Passive electrical properties of cell membranes from Whole-cell patch-clamp recordings at day 80.